NeuroImage 202 (2019) 116023

Contents lists available at ScienceDirect

NeuroImage

journal homepage: www.elsevier.com/locate/neuroimage

Functional connectivity of brain associated with passive range of motion exercise: Proprioceptive input promoting motor activation?

Fatima A. Nasrallah [a,e], Abdalla Z. Mohamed [a], Megan EJ. Campbell [a], Hong Kai Yap [b], Chen-Hua Yeow [c], Jeong Hoon Lim [d,*]

[a] Queensland Brain Institute, The University of Queensland, Brisbane, QLD, 4072, Australia
[b] Singapore Institute of Neurotechnology and Advanced Robotics Center, Singapore
[c] Department of Biomedical Engineering, National University of Singapore, 117583, Singapore
[d] Department of Medicine, Yong Loo Lin School of Medicine, National University of Singapore, 119228, Singapore
[e] Clinical Imaging Research Center, National University of Singapore, Singapore

ARTICLE INFO

Keywords:
Functional magnetic resonance imaging
Soft actuators
Soft wearable robotics
Tactile stimulation
Proprioceptive stimulation

ABSTRACT

Soft robotics have come to the forefront of devices available for rehabilitation following stroke; however, objective evaluation of the specific brain changes following rehabilitation with these devices is lacking. In this study, we utilized functional Magnetic Resonance Imaging (fMRI) and dynamic causal modeling (DCM) to characterize the activation of brain areas with a MRI compatible glove actuator compared to the conventional manual therapy. Thirteen healthy volunteers engaged in a motor-visual fMRI task under four different conditions namely active movement, manual passive movement, passive movement using a glove actuator, and crude tactile stimulation. Brain activity following each task clearly identified the somatosensory motor area (SMA) as a major hub orchestrating activity between the primary motor (M1) and sensory (S1) cortex.

During the glove-induced passive movement, activity in the motor-somatosensory areas was reduced, but there were significant increases in motor cortical activity compared to manual passive movement. We estimated the modulatory signaling from within a defined sensorimotor network (SMA, M1, and S1), through DCM and highlighted a dual-gating of sensorimotor inputs to the SMA. Proprioceptive signaling from S1 to the SMA reflected positive coupling for the manually assisted condition, while M1 activity was positively coupled to the SMA during the glove condition. Importantly, both the S1 and M1 were shown to influence each other's connections with the SMA, with inhibitory nonlinear modulation by the M1 on the S1-SMA connection, and similarly S1 gated the M1-SMA connection. The work is one of the first to have applied effective connectivity to examine sensorimotor activity ensued by manual or robotic passive range of motion exercise, crude tactile stimulation, and voluntary movements to provide a basis for the mechanism by which soft actuators can alter brain activity.

1. Introduction

Passive range of motion exercise of joints in the paralyzed extremity is a very basic therapy in neurorehabilitation. This intervention can mobilize the paretic limbs and induce re-growth of neural circuitry, which would eventually aid recovery through neuroplasticity (Jack et al., 2001). In the past decade, there has been a major surge in the adoption of soft robotic actuators (Godfrey et al., 2018; Haghshenas-Jaryani et al., 2016; Koh et al., 2017; Tarvainen et al., 2018) which can replace or supplement conventional manual therapy to provide passive joint mobilization continuously for successful rehabilitation outcome. However, there is a paucity of research examining the real-time effects of exercise therapy on brain function to investigate further the mechanism. On top of that, characterization of such robotic actuators in the activation of brain areas compared with conventional manual therapy has not been elucidated sufficiently due to technical challenges in illustrating the neurophysiological or functional activity.

Functional MRI is an advanced imaging method that allows the spatial mapping of the different circuitry of the brain noninvasively. MR-glove (Yap. et al., 2017) is a MRI-compatible soft robotic glove, devoid of metallic components, which enables mapping brain function on a real time basis while carrying out motor/sensory tasks. To probe the neural networks that are involved during brain activation, of significant importance is the understanding of: 1) the motor and sensory interaction

* Corresponding author.
E-mail address: jeong_hoon_lim@nuhs.edu.sg (J.H. Lim).

https://doi.org/10.1016/j.neuroimage.2019.116023
Received 15 November 2018; Received in revised form 7 June 2019; Accepted 15 July 2019
Available online 17 July 2019

in inducing invariant sensory stimulation and structuring sensorimotor function and 2) the need of self-organization mechanisms to digest and structure the information brought forward by a number of sensory and motor elements.

Integral to this sensory and motor network is the supplementary motor area (SMA) which is a region localized in the posterior part of the superior frontal gyrus (Penfield and Welch, 1951). The SMA is an area with rich connections to both cortical and subcortical structures (Dum and Strick, 1991; Maier and Remus, 2002; Mitz and Wise, 1987; Murray and Coulter, 1981). Furthermore, the SMA is embedded in motor circuits through its connections with the primary motor cortex, premotor cortex, and cingulate cortex (Luppino, 1993). Dorsal anterior cingulate cortex is known to undergo task-related undirected functional coupling with both the SMA and primary motor cortex (M1), but sends task-specific directed signals specifically to the SMA (Asemi et al., 2015) which has connections to the insula (Luppino et al., 1993), basal ganglia (Inase et al., 1999), cerebellum (Akkal et al., 2007), thalamus (Behrens et al., 2003) posterior parietal lobe (Zhang et al., 2012), and contralateral SMA (Liu et al., 2001). Qualitatively, the anterior and posterior portions of the SMA appear to be engaged in different types of tasks such as sensory, speech expression, and memory (Chung et al., 2005). SMA is modulated by the interactive effects of proprioceptive and efference copy based information (Stock et al., 2013). When SMA is damaged structurally, it may entail a global akinesia, predominantly on the contralateral side, mutism while preserving muscle strength (Potgieser et al., 2014).

In work conducted by Bishop et al., 11 regions have been shown to comprise the sensorimotor network (Bishop, 2014). Many of these nodes such as the SMA, PMC, M1, Cerebellum, and S1 are considered to be relevant to the sensorimotor network as shown by previous literature (Kuhtz-Buschbeck et al., 2008; Grefkes et al., 2010; Bardouille and Boe, 2012). Furthermore, the SMA had the highest node degree with a degree of 13. In a study investigating voluntary movement, Orgogozo et al. (Orgogozo and Larsen, 1979) showed that during motor activity, there was an increase in cerebral blood flow to the SMA in addition to the sensorimotor cortex. However, during the mental counting task, blood flow was not increased to the SMA, highlighting its importance to tasks that require movement, irrespective of complexity. Several other studies have confirmed the central role of the SMA in movement using MEG (Pollok et al., 2004) and fMRI (Floyer-Lea and Matthews, 2004; Bardouille and Boe, 2012). Xu et al. (Xu et al., 2014), examined the differences in the neural networks produced from a motor execution task (unilateral dominant UL) and a motor imagery task, using functional connectivity fMRI (fcMRI). Using only 13 ROIs, the authors conclude that the SMA is the only hub or 'key' node within the motor execution network in their study. Finding the SMA as a hub coincides with the present study.

We hypothesized that the sensory inputs elicited by a passive range of motion exercise may modulate SMA to provide signals to activate primary motor cortex subsequently. In this work, we utilized the MRC-glove enabling continuous flexion/extension of fingers by a pneumatic controller to produce passive proprioceptive stimulation in a magnetic field. For the comparison, we applied manually actuated proprioceptive activation simulating conventional physiotherapy, active voluntary visuomotor control and tactile sensory activation. We investigated functional relations of the motor network by mapping the network correlations between the SMA, primary somatosensory cortex (S1) and M1 using undirected analysis of the fMRI Blood-Oxygen-Level-Dependent (BOLD) time series data. To assess modulatory signaling from the SMA to M1, we used effective connectivity analysis using nonlinear dynamic causal modeling which measures the influence of one brain area on that of another area.

2. Materials and method

2.1. Participants

Thirteen healthy right-handed volunteers (mean age of 25.7 ± 17.25 [$n = 9$ males, mean age 35.6 ± 16.8 and $n = 4$ females, mean age is 35.75 ± 20.87]) participated in the study. Inclusion criteria comprised no previous record of joint injuries or deformities, no previous history of stroke, spinal cord injury, or muscular dystrophy, and healthy status with BMI between 18.5 and 24.9. Exclusion criteria included being overweight, hand injuries, permanent metallic implants (such as pacemaker, surgical clips, dental braces, metal ear implants, history of metal fragments in eyes) and subjects who did not wish to be photographed or recorded. All participants were right-handed. This study was approved by the National Healthcare Group Domain Specific Review Board and informed consent were obtained from all patients.

2.2. Study design

To assess the effect of a self-assisted soft-robotic actuator on the brain, we conducted a randomized functional MRI study where participants were involved in four separate functional MRI interventions: 1) Active: voluntary flexion/extension of fingers following the paradigm, 2) Manual passive: manual flexion/extension of fingers by an assistant with holding patient's fingers, 3) Sensory: crude touch of hand dorsum manually by an assistant, and 4) Glove passive: Continuous automatic passive flexion/extension of fingers (0.1 Hz) by a soft robotic actuator. A full validation of the soft robotic glove, MR-glove, has been published in our recent study (Yap et al., 2017; refer to schematic in Fig. 1).

2.3. MRI data acquisition

MR scans were performed on a 3T Tim Trio scanner (Siemens, Germany) with a 32 channel head array coil. Subjects lay supine in the scanner with a rubber bulb in each hand and resting in custom hand supports to prevent movement. A T1-weighted anatomical image was acquired with a magnetization prepared rapid gradient-echo (MPRAGE) sequence with the following parameters: TR = 1900 ms, TI = 900 ms, TE = 2.52 ms, FOV = 256 × 256, flip angle = 8, number of slices = 176, voxel size = 1 mm isotropic, and slice thickness = 1 mm. Functional MRI data were acquired using a single shot Echo Planar Imaging (EPI) sequence using the parameters: TR = 3000 ms, TE = 35 ms, FOV = 182 × 182, voxel size = 3.4 mm isotropic, and number of measurements = 89. Data acquisition was carried out during a visual-attention motor task where the subjects were asked to close and open their hand during the paradigm. The paradigm consisted of an 18 s rest followed by 5 active blocks of 30 s each interleaved with 21 s rest and then ended with 18 s rest. In each 30 s active block, the task was a dynamic finger flexion and extension cued by a visual stimulus of a moving hand. Both the flexion and extension time were 3 s. The guidance cue instructed subjects to close or open their corresponding hand according to the cue. Functional scans were performed for each of the left and right hands. The same paradigm was applied to all the conditions tested. The conditions were randomized for every subject. In the Active task, subjects actively and voluntarily followed the cues on the screen. In the Glove passive task, flexion/extension of the glove was controlled by a custom written script that was synced to the paradigm and was therefore automatically triggered by the paradigm and scanner. A custom written script controlled both the onset and frequency of flexion/extension of the glove according to the paradigm. The Manual passive task, on the other hand, was initiated by an assistant who stood by the subject and followed the task cues by moving the subjects hand in line with the paradigm prompts. The same paradigm was followed for the Sensory task only that in this instance the assistant performed sensory touch of the hand dorsum in line with the cues presented. The assistant was holding a timer to control the frequency (1 Hz) of the sensory touch.

2.4. Data processing and analysis

Data pre-processing and analysis were performed using the FMRIB's Software Library (Jenkinson et al., 2002; FSL 5.0.9, Analysis Group, FMRIB, Oxford, UK, www.fmrib.ox.ac.uk/fsl), and FreeSurfer (Fischl,

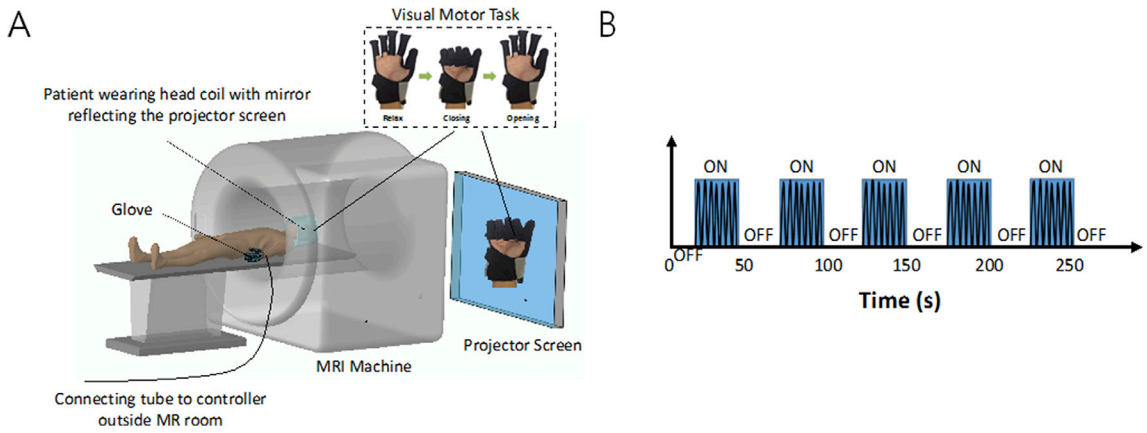

Fig. 1. A schematic diagram of the study design. (A) In the MRI scanner, participants engaged in a visual motor task which comprised a dynamic finger flexion and extension cued by a visual stimulus of a moving hand. In each stimulation block, the guidance cue instructed subjects to close or open their corresponding hand according to the guidance cue. Participants wore the glove in their corresponding hand during glove passive task. **(B)** A schematic representation of the paradigm used which comprised 18 s rest followed by 5 active blocks of 30 s each interleaved with 21 s rest and then ended with 18 s rest with each block comprising repeated hand closing-opening motions. Each task was performed twice, once for the right hand and once for the left hand.

2012; Martinos Center for Biomedical Imaging, Laboratory for Computational Neuroimaging, Boston, United States).

Each fMRI run was corrected for slice timing (FSL-slicetimer), head motion (FSL-MCFLIRT; Jenkinson et al., 2002), and skull stripped (FSL-BET; Smith, 2002). Scans with head movement more than 1.5 mm were excluded (Caparelli et al., 2003) to avoid any influence of head movement on the results. The skull-stripped, intensity corrected T1 structural images and fMRI runs were then resampled to a voxel size of $2 \times 2 \times 2\ mm^3$ and linearly co-registered to each other using FreeSurfer's bbregister tool (Greve and Fischl, 2009) that used the cortical surface reconstruction to improve structural-functional MRI co-registration. The individual's T1 image was then normalized to the standard Montreal Neurological Institute (MNI) template linearly using FMRIB's linear co-registration tool (FLIRT) (Jenkinson et al., 2002; Jenkinson and Smith, 2001) and non-linearly using FMRIB's nonlinear co-registration tool (FNIRT) generating warp files used to register fMRI runs to MNI. fMRI data were then spatially smoothed using a Gaussian kernel of full width at half maximum (FWHM) = 6 mm to decrease spatial noise.

To generate individual voxel-wise statistical parametric maps of brain activity representing each task in contrast to rest condition, we used the general linear model (GLM). For each participant, we constructed the GLM design matrix by modeling the regressors for each task as described in Fig. 1. These task-regressors were convolved with a canonical hemodynamic response function to generate an estimate response function for each task. We fed our GLM a design matrix for each task, including task hemodynamic responses, six rigid parameters of motion artifacts, average time courses of the white matter, and average time courses of ventricles. The resulted individual maps were assessed to make sure that the pattern of functional activity is matching with the experimental paradigm.

Group average maps for contrast images of each task (Active-rest, Glove-rest, Manual-rest, Sensory-rest) in each group were computed as one sample group averages using a mixed effects statistical model (FLAME, Feat, FSL). To assess the differences in brain activation between different tasks (i.e. Active Right vs Glove Right, Active Left vs Manual Left, etc.), we calculated voxel-based paired t-tests (within subjects) in each group using a mixed effect model (FLAME, Feat, FSL) for each task. All statistical analysis maps were corrected for age and gender as confounding factors and corrected for multiple comparisons using family-wise correction ($\alpha < 0.05$).

2.5. Dynamic causal modeling of effective connectivity

A post-hoc series of hypotheses were designed to examine the task-related modulation of effective connectivity within a core sensorimotor network. These hypotheses were focused specifically on BOLD-signal changes for Glove versus Manual passive movement conditions (right-hand only), and aimed to explain the unique engagement of the SMA during the Manual-R condition. Dynamic causal modeling (DCM) requires user-specified regions of interest (ROI) to form the 'nodes' of hypothesized networks with different configurations of connectivity and interaction (Friston et al., 2003; Kahan and Foltynie, 2013; Stephan et al., 2010). These ROIs are defined based on the results of the group-level GLM analysis (see below, Results section) and *a prior* knowledge of the structure and function of these areas. Based on the group analysis described above, for the specific effects of interest from Manual > Glove for the right-hand, we selected five ROIs from peak-voxels within the SMA (MNI coordinate: 2, −16, 62), left and right M1 (left: 32, −16, 62; right: 30, −16, 62) and left and right S1 (left: 40, −32, 54; right: 40, −32, 62). Each ROI was defined as 5 mm spheres around these group-level peaks, with adjustment for the individual subject's local maxima. We constrained coordinate adjustment to subject-specific local maxima within each anatomical area of interest as defined by Human Motor Area Template (Mayka et al., 2006). A separate subject-level GLM was conducted with SPM12 (n = 13, controls) for just these two task conditions of interest (Glove-R and Manual-R, versus rest). From this reduced GLM, we then extracted the subject-level time-series of task-related signal--change within each ROI. These time-series were used as inputs to DCM so as to assess the mechanisms for sensorimotor integration underlying the two passive movement conditions.

The models were based on five ROIs that are known to be highly interconnected (Mayka et al., 2006), including interhemispheric connections between both S1 and both M1 nodes. Hence our network was designed with bidirectional connections between all five nodes. This configuration was validated by comparing three structural models (without any task-related modulation or driving input): 1) fully-connected; 2) all but direct S1-M1 connections with just the SMA node being fully connect to the other 4 nodes and; 3) all but direct connections across hemispheres between left S1 and right M1 or right S1 to left M1 (Fig. S1). Despite penalties for complexity in the model selection process, the most complex, fully-connected design was 99% more likely to fit the data than the other two more restricted designs.

This fully connected network then formed the base template of all eight DCMs in our constrained model-space (Fig. 6). These were further divided as two 'families' of sets of four models. Each of these four designs varied by one key aspect: the nonlinear modulation of effective connections to the SMA. Nonlinear modulation is simply the influence of the activity of one region on the communication between two other regions

(Stephan et al., 2008). Crucially nonlinear DCM incorporates this aspect of modulation of connectivity by a specific neural population, reflecting a neurobiological mechanism for neural gain control; whereas, in bilinear models the source of this kind of modulation is unspecified (Stephan et al., 2008; Breakspear, 2013).

Our nonlinear designs tested for the interactions between the activity of the left S1 and M1 regions, and the connections to SMA (self-connections or incoming connections from other network nodes). These are depicted in Fig. 6, with the "Sensory" hypotheses (Fig. 6A, C) being that S1 exerts nonlinear modulation (gating) of connections to the SMA, whereas the "Motor" hypotheses (Fig. 6B, D) proposes that the M1 exerts nonlinear modulation on these SMA connections. Next, we specified two designs for driving inputs which represented externally driven neural changes, here resulting from our two passive movement tasks (Friston et al., 2003). In Fig. 6 the 'dual-input' design is shown, with both the S1 and M1 receiving task-related driving inputs, i.e. both sensory and motor representations were generated from both the tasks. This dual input node design was incorporated into the first four models proposed (models 1 to 4, Fig. 6A and B) and constituted one model family. For the second half of the model-space (6–8), the design was posed such that only the S1 received direct driving inputs and thus the M1 received signals only via sensory representations of the task ('single-input' family, Fig. 6C and D).

Finally, the specifications for the task-dependent modulation of connectivity between regions were kept constant across all models (Fig. 6). This was informed by the group-level analysis highlighting broader engagement of sensory areas in the Manual-R condition, while more prominent motor cortex engagement was observed in the Glove-R. We specified the modulation of connections between M1 and SMA and left-right M1 regions by Glove-R, hypothesizing a greater motor response in this condition. The Manual-R condition was hypothesized to involve a greater sensory response, and so, we modelled this condition as modulating the S1-SMA connection and left-right S1 connection.

The second stage of DCM analysis, Bayesian model selection (BMS), is data driven and uses a Bayesian approach to estimate the likelihood that the model fit for one model exceeds that of all other models in the model-space (Rigoux et al., 2014). BMS applies a penalty for complexity (preference for most parsimonious model) while selecting the model which best accounts for the data (Stephan et al., 2009). RFX addresses heterogeneity or outliers within the group (Penny et al., 2010), and this second level analysis (the key BMS result reported here) is the 'exceedance probability' and allows for model-space partitioning to compare subsets of models – here we employed this to compare dual versus single-input designs. The family or model with the highest exceedance probability is considered as 'winning' relative to the other models tested, it is most likely to explain the observed fMRI effects. Here we applied a two-stage model-selection procedure: firstly comparing two families to select the best design for driving-inputs (dual or single nodes, Fig. 6A and B versus C,D); and secondly, comparing all individual models to examine the central hypotheses regarding indirect modulation of SMA connections by either M1 or S1 influence (termed 'motor' or 'sensory' hypotheses, respectively, Fig. 6). In this way we confirmed the model features most relevant to our hypotheses. Finally, Bayesian Model Averaging can be useful to delineate between models that perform similarly (as was the case here) and provide parameter estimates for coupling and modulation of connectivity which accounts for this uncertainty across the model-space (Stephen et al., 2010).

3. Results

As mentioned in the "Study Design" section, four different conditions were investigated during functional MRI for both left and right hands: 1) Active task: where subjects actively/voluntarily performed flexion and extension of fingers following cues in the fMRI paradigm, 2) Manual passive task: where subjects performed manual flexion and extension of fingers that was aided by another assistant who followed the cues, 3) Sensory task: where an assistant performed crude touch of the hand dorsum manually in line with the cues presented during the task, and 4) Glove passive task: where subjects underwent continuous passive flexion and extension of fingers that was automatically controlled by a pneumatic controller.

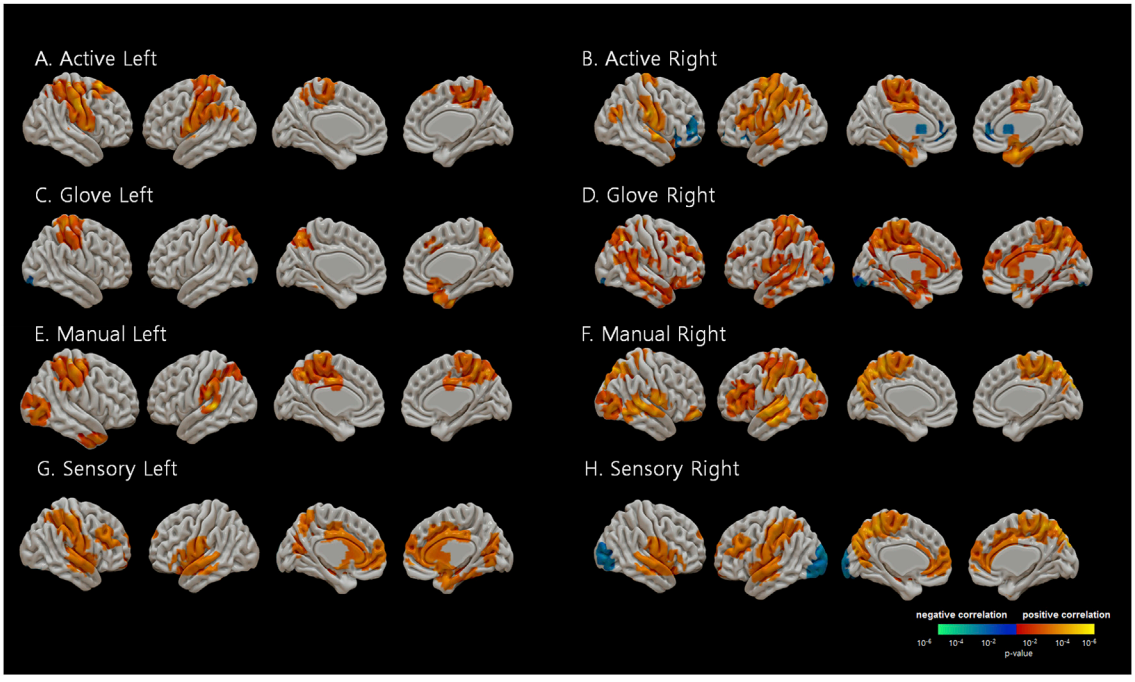

Fig. 2. Rendered group functional MRI maps of activated regions of the brain. Participants underwent a visual-motor task under four different conditions: **(A)** left Active and Right Active, **(B)** Left Glove and Right Glove, **(C)** Left Manual and Right Manual, **(D)** Left Sensory and Right Sensory performed by healthy participants. Red-yellow represents the positive activity in relation to the task paradigm and blue-green represent negative activations in relation to the task paradigm. These group average maps were corrected using false discovery rate correction with a< 0.05.

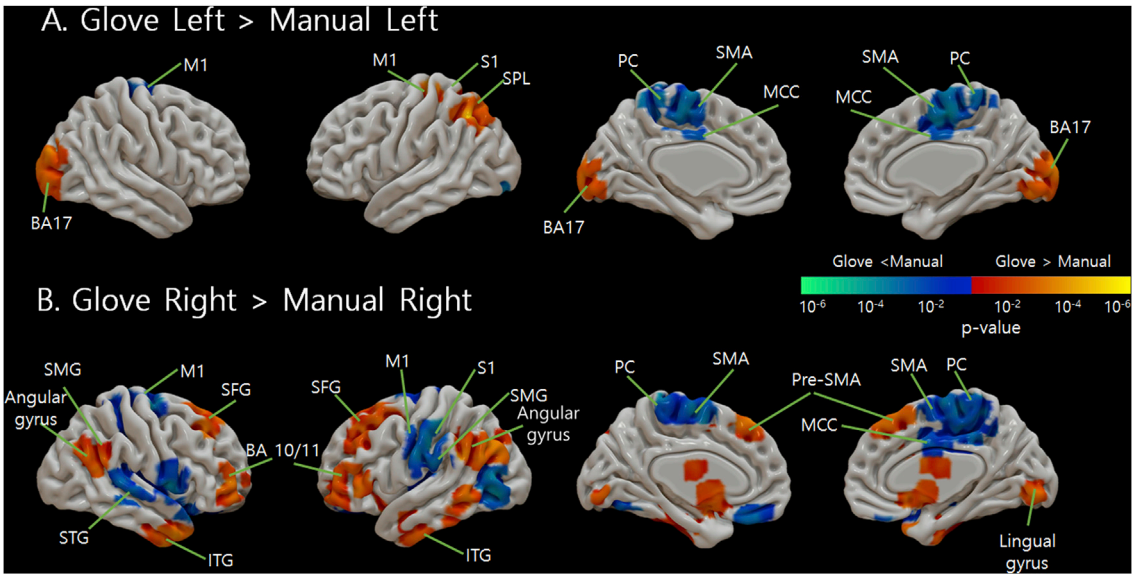

Fig. 3. Group Average maps of functional MRI data representing areas of increased/reduced activity between Glove-assisted movement and movement performed by another person assistance (Manual) (A) of the left hand and (B) Right hand. Red-yellow represents higher activity in the Glove task in contrast to Manual task, while blue-green represents higher activity in Manual task as compared to Glove Task. These group difference maps were corrected for multiple comparisons using false discovery rate (a< 0.05) with a cluster-thresholding method with $z > 2.3$ and $p < 0.05$.

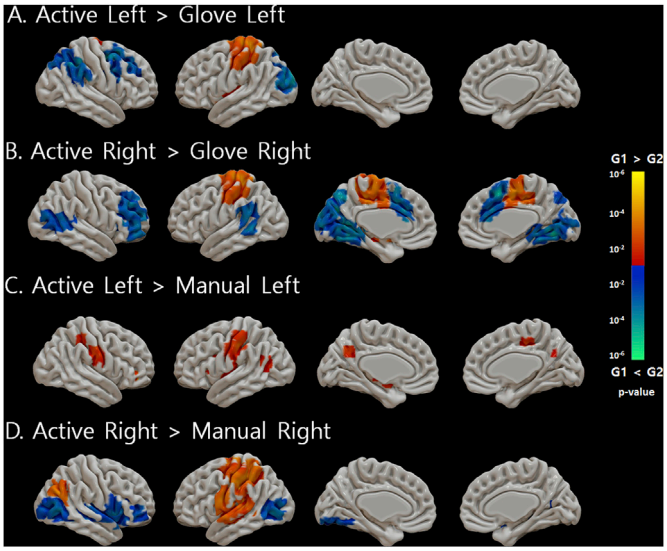

Fig. 4. Group difference maps for functional MRI data representing areas of differences between active and passive movement conditions. (A) Active Left movement versus Glove-assisted Left **(B)** Active Right versus Glove Right **(C)** Active Left versus Manually-assisted Left **(D)** Active Right versus Manual Right. Red-yellow represents higher activity in the voluntary active condition as compared to glove or manual passive movement, while blue-green represents higher activity in glove or manual passive movement as compared to voluntary active condition. Comparisons were performed using paired *t*-test and the resulted group difference maps were corrected for multiple comparisons using false discovery rate ($\alpha < 0.05$) with cluster-thresholding method with $z > 2.3$ and $p < 0.05$. G1 refers to Task 1 in comparison and G2 refer to Task 2 on the color bar.

3.1. BOLD activation of the motor network during active, manual passive, glove passive, and sensory tasks

Fig. 2 represents the group average statistical maps representing the brain BOLD activity following each fMRI task intervention. In the Active left, a significant increase in the BOLD signal activation was seen in the bilateral primary motor cortex (M1), primary sensory cortex (S1), supplementary motor area (SMA), auditory cortex, and insula; right Superior frontal gyrus (SFG), and left supramarginal gyrus (SMG), and superior temporal gyrus (Fig. 2A). The active right task showed similar activations, but with the peak activity in M1 and S1 located in the left hemisphere with patterns of increases in BOLD activity located in the bilateral M1, S1, SMA, insula, SMG, middle cingulate cortex (MCC), medial temporal lobe, and hippocampus, along with left premotor, and right angular gyrus (Fig. 2B). The glove passive left task showed BOLD activity in right M1, right S1, right anterior cingulate cortex (ACC), bilateral precuneus, and left superior parietal lobule (SPL) (see Fig. 2C). Glove passive right task showed more BOLD activity located at left M1, left S1, left insula, bilateral MCC, ACC, middle frontal gyrus (MFG), precuneus, dorsolateral prefrontal cortex (DLPFC), SMG, angular gyrus, SMA, orbitofrontal gyrus, and superior and middle temporal gyrus (STG, MTG) (see Fig. 2D). The manual passive left activated the right M1, S1, MTG, ITG, middle and inferior occipital gyrus, the bilateral SMA, MCC, SMG, precuneus, and SPL (Fig. 2E); while the right manual passive task activated the left M1, S1, left middle and inferior frontal gyrus, and orbitofrontal gyrus, along with bilateral SMA, precuneus, STG, MTG, SPL, middle and inferior occipital gyrus, and insula (Fig. 2F). The sensory left task activated the bilateral S1, auditory cortex, STG, MTG, ACC, MCC, medial frontal gyrus, cuneus, precuneus, caudate, and putamen, and right medial temporal cortex, and MFG (Fig. 2G), while right sensory task activated left S1 and cuneus, bilateral auditory cortex, SMA, STG, MTG, ACC, medial frontal gyrus, and precuneus, and MFG with decreased activity in bilateral middle and inferior occipital gyrus (Fig. 2H).

3.2. BOLD activity during glove activation and manual passive exercise

When comparing between Glove assisted passive movement and manual assisted movement, we were able to identify the differences in the neural components involved in both tasks. Interestingly, the glove passive task showed reduced bilateral paracentral cortex, MCC, and SMA as compared to manual passive task using both right and left hands; and left M1 for left hand movement, and bilateral M1, S1, insula, inferior occipital gyrus activity for right hand as compared to manual passive task (Fig. 3A and B). Furthermore, we observed increased activity in the glove passive task as compared to the manual passive task in left M1, S1, SPL,

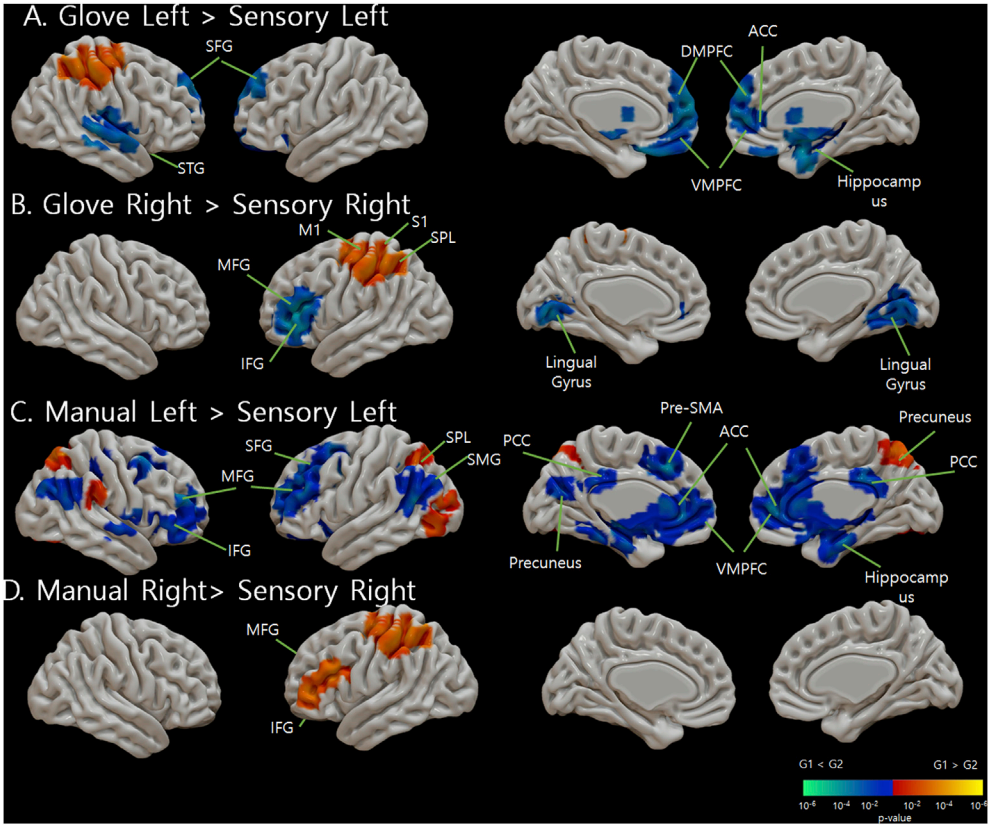

Fig. 5. Group Average maps of functional MRI data representing areas of increased/reduced activity between passive and sensory conditions. (A) Glove-assisted left compared to sensory left, **(B)** glove right versus sensory right, **(C)** Manual left versus sensory left, and **(D)** Manual left versus sensory right. Red-yellow represents higher activity in the glove or manual in contrast to Sensory, while blue-green represents higher activity in sensory task as compared to glove or manual. Comparisons were performed using paired *t*-test and the resulted group difference maps were corrected for multiple comparisons using false discovery rate ($a < 0.05$) with cluster-thresholding method with $z > 2.3$ and $p < 0.05$. G1 refers to Task 1 in comparison and G2 refer to Task 2 on the color bar.

and lingual gyrus (BA 17) for the left hand; and in bilateral pre-SMA, lingual gyrus, SFG, insula, middle and inferior frontal gyrus (BA10/11), STG, ITG, and thalamus for the right hand (Fig. 3A and B).

3.3. BOLD activities in glove passive and manual passive task are different as compared to voluntary motor task

When comparing between voluntary movement task, and both glove assisted passive movement and manual assisted movement, we were able to identify the differences in the neural components involved in both voluntary and assisted movement tasks. The active left task showed increased activity in the left M1, S1, SPL, insula as compared to glove left and showed decreased activity in right premotor, middle frontal gyrus, SPL, SMG, and left superior and middle occipital gyrus (Fig. 4A). Compared to glove right, active right showed increased activity at the bilateral SMA, and left M1, S1, and SPL; while showed decreased activity in bilateral pre-SMA, ACC, precuneus, cuneus, and lingual gyrus, along with left SMG, and right middle frontal gyrus, inferior frontal gyrus, and orbitofrontal gyrus (Fig. 4B).

Furthermore, as compared to manual left, active left showed increased activity at the bilateral S1, and precuneus, and in left M1, SMG, and insula along with right MCC (Fig. 4C). Compared to the manual right, active right showed increased activity at the left M1, S1, SPL, STG, SFG, SMG, insula, and premotor along with right angular gyrus, while showed decreased activity in bilateral middle and inferior occipital gyrus, and left lingual and fusiform gyrus (Fig. 4D).

3.4. BOLD activities in glove passive and manual passive task are different as compared to sensory task

We showed in Fig. 5 the differences in BOLD activity between the glove and manual passive tasks and the sensory tasks to identify the non-sensory components contributing to their pattern of activation. Compared to left sensory task, glove passive left showed increased activity in right M1, S1, premotor, and SPL, while showed decreased activity at bilateral SFG, DLPFC, and ACC, and right STG (Fig. 5A). Furthermore, compared to right sensory, glove assisted right showed increased left M1, S1, SPL and premotor, and showed decreased activity in the bilateral lingual gyrus, left MFG, and left IFG (Fig. 5B).

In contrast to the left sensory task, the left manual passive task showed decreased BOLD activity in bilateral ACC, VMPFC, SFG, SMG, angular, STG, and posterior cingulate cortex (PCC), and right S1, while the increased BOLD activity was observed in the superior parietal lobule, middle and inferior occipital gyrus, and precuneus (Fig. 5C). Furthermore, the right manual passive task showed increased BOLD activity in left M1, S1, SPL, middle and inferior frontal cortex (Fig. 5D) compared to the right sensory task.

3.5. Dynamic causal modeling of the sensorimotor network

Comparing the models at the family level showed that neither the dual-input family nor the family of single-input models were particularly more likely than the other, with family-wise exceedance probabilities of 52.1% and 47.9% respectively. Moving to model-wise BMS, we highlighted two models out of the eight specified as close competitors: models number 6 and 7. However, again estimates of model evidence were not able to clearly delineate a 'winning' model as both model 6 and 7 being similarly likely to outperform the rest of model-space by 25.8% and 26.2% respectively. Furthermore the Bayesian Omnibus Risk (BOR) for out model-space indicated that the risk of a type 1 error was very high, with a 91.2% chance that in fact all models were equally likely (Rigoux et al., 2014). This high BOR is also indicated by the protected exceedance probabilities, a more conservative estimate of model likelihood which by accounting for the BOR quantifies the probability that any one model is actually more likely than the others beyond chance. The exceedance and protected exceedance probabilities for each model are plotted in Fig. 7A, with protected probabilities showing that the likelihood of any model winning beyond chance was consistently low for all models (12–15%).

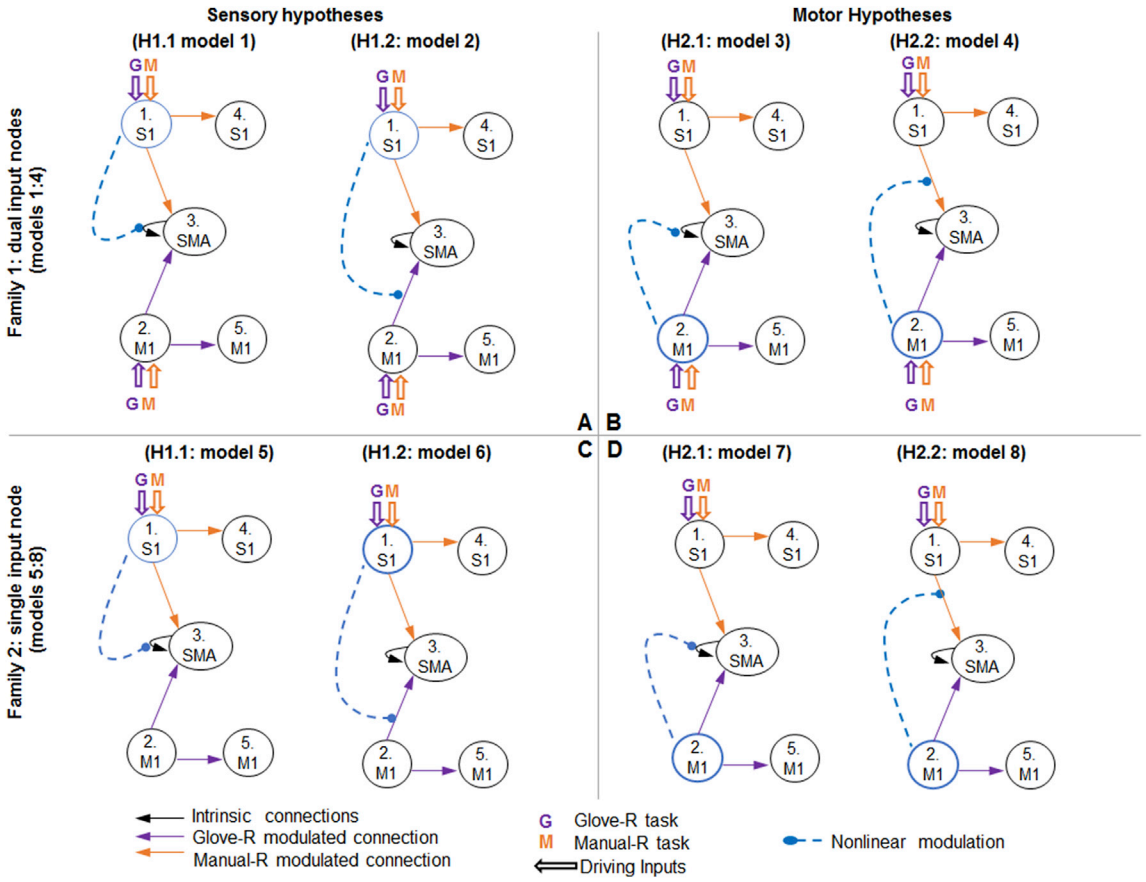

Fig. 6. Model-space of 8 Dynamic Casual Models built by combining several design aspects for modulation and driving inputs. Model-space of 8 DCMs built by combining several design aspects for modulation and driving inputs. Shows Families 1 (models 1–4, panels A & B) and 2 (models 5–8, panels C & D) which have alternatives for the driving inputs of Glove (G) and Manual (M) right-handed passive movement conditions. Vertically the models are divided into "Sensory Hypotheses" (A & C) for nonlinear modulation of SMA connections by S1 (1.1. for models 1 & 5; 1.2 for models 2 & 6), versus the "Motor Hypotheses" (B & D) for nonlinear modulation of SMA connections by M1 (2.1. for models 3 & 7; 2.2 for models 4 & 8). The task-related modulations of G and M conditions on the intrinsic connections between regions was kept constant across all eight models. *Note:* for ease of displaying our modulatory hypotheses, only those intrinsic connections that were the hypothesized to be modulated are displayed, however the models were specified with all nodes being bidirectionally connected to each other, as per the 'fully connected' configuration in Fig. 6.

Nevertheless, the two top-performing models both belonged to the single-input family in which only the left S1 received driving inputs from the task stimuli for right-hand Glove and Manual passive movements. Given this Bayesian Model Averaging (BMA) was employed to estimate the model parameters of the strongest features of our model-space. Again, BMA accounts for the uncertainty of a model-space in estimating coupling and modulating parameters of the model network, adjusting these in line with the likelihood of the individual model features.

The results of BMA produced a set of parameters which captured the features of two nonlinear hypotheses with a single-input design: models: H1.2 where the left S1 modulates the left M1 to SMA connection strength; and H2.2 with the left M1 modulating connection of left S1 with the SMA. The estimates for intrinsic connections (A-matrix) are provided in Table 1. The estimates for task-related modulation, and driving inputs are shown in Fig. 7B, while panel C shows the estimates of nonlinear modulation of incoming connections with the SMA. This combination model implicates a dual-gating of sensory and motor inputs to the SMA. The positive (excitatory) connectivity between left S1 and SMA being upregulated by the Manual condition (Fig. 7B), but then with the primary motor area reducing this S1-SMA coupling (−6.7%). The primary somatosensory cortex had negative (inhibitory) intrinsic connectivity with SMA, which the Glove condition increased (greater inhibition signal), while nonlinear modulation of by the left S1 reduced the coupling strength between M1-SMA (−7.9%).

4. Discussion

To the best of our knowledge, this is the first paper to compare the brain responses ensued by manual or robotic passive range of motion exercise, crude tactile stimulation, and voluntary motor activation on a real time basis. This study utilized a motor-visual fMRI task to investigate the activation of sensory and motor brain areas and implemented dynamic causal modeling to understand the causal inferences of the brain circuitry involved in such stimulation.

4.1. Functional MRI findings following motor-sensory activation

Based on fMRI findings, active voluntary movement showed a significant increase in the BOLD signal in the contralateral M1, S1 and SMA (Figs. 2A and 3A). The robotic passive proprioceptive stimulation activated the contralateral M1, S1, SMA and the posterior cingulate (Figs. 2B and 3B). The manual passive joint exercise preferentially activated the posterior cingulate, and S1 in the corresponding hemispheres (Figs. 2C and 3C). On the other hand, the sensory task, crude touch, activated S1 and SMA but not M1 (Fig. 2D). These findings are consistent with a previous study showing that proprioceptive processing is important for appropriate motor control, providing error-feedback and internal representation of movement for adjusting the motor command (Cignetti et al., 2017). The unique engagement of the SMA and M1 during the manual passive and glove passive condition, not during crude tactile stimulation,

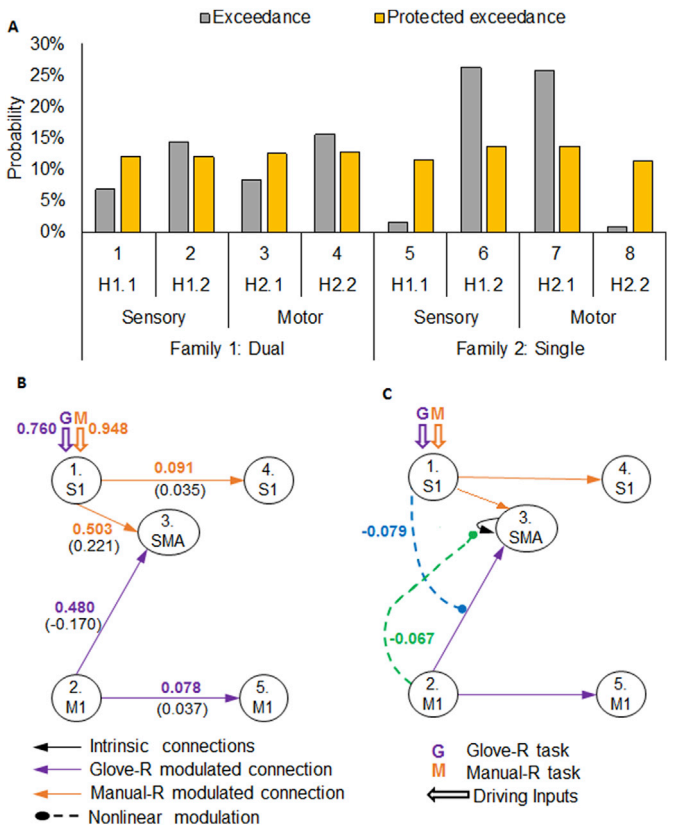

Fig. 7. Bayesian Model Selection from a model-space of 8 dynamic causal models of effective connectivity. (A) Comparison of all eight models with the exceedance probability (xp) plotted for each model. Highlighted in green is the best performing model: dual-design with the sensory hypothesis (H1.2) of the S1 gating the inputs from M1 to SMA. **(B)** Mean parameter estimates of the strength of driving inputs by task conditions and of the task-related perturbation of connectivity (Glove and Manual task-related changes indicated by purple and orange numbers respectively). The values in brackets are the intrinsic coupling parameter for that connection, for the details of all estimates of intrinsic coupling parameters see Table 1. **(C)** Mean parameter estimates for the nonlinear modulation of the left M1-SMA connection by S1 (Model 6: Hypothesis 1.2, blue dashed line), and by left M1 on to SMA self-connections (Model 7, hypothesis 2.1, green dashed line). *Note:* all parameters were obtained by Bayesian model averaging (BMA) as the results of BMS were inconclusive given the BOR: 0.9119 and similar probabilities for the two top performing models.

Table 1
Bayesian Model Averaged estimates for intrinsic coupling parameters within our fully-connected network. Negative values imply an inhibitory connection and positive values an excitatory connection.

To:	From:				
	1. left S1	2. left M1	3. left SMA	4. right S1	5. right M1
1. left S1	−0.122	−0.602	0.034	0.107	0.104
2. left M1	0.533	−0.114	0.172	0.039	−0.050
3. left SMA	0.221	−0.170	−0.031	−0.003	0.048
4. right S1	0.035	0.017	0.025	−0.091	0.106
5 right M1	0.072	0.037	0.010	0.119	−0.094

supports our hypothesis that proprioceptive inputs elicited by passive range of motion exercise may modulate SMA to provide signals to primary motor cortex. Given that SMA is a region with rich connections to both cortical and subcortical structures and is modulated by the interactive effects of sensory input and efferent signal (Stock et al., 2013), various interventions such as active voluntary movement, passive proprioceptive stimulation and crude tactile stimulation were expected to induce significant SMA activation.

The finding that manual passive task and sensory task, crude touch, activated S1 more than glove passive task (Fig. 5) is understandable as both of manual passive task and crude tactile stimulation were carried out by an assistant hand with holding the subject's fingers while glove passive task was done by a soft actuator wrapping fingers. Manual passive task might have produced a significant amount of tactile stimulation when holding the subject's fingers to repeat flexion and extension on top of proprioceptive stimulation. As such, manual passive task should have exerted more intense influence on S1 and SMA than glove passive task.

4.2. *Effective connectivity of the motor circuitry*

The interactions based on effective connectivity amongst ROIs, SMA, M1 and S1, were further explored with probing the unique engagement of the SMA and M1 during the manual passive and glove passive condition. As shown in (Fig. 6), we placed the driving inputs of glove passive and manual passive task conditions, as either exclusively to S1 or to both of M1 and S1. While the SMA was not modelled as receiving driving inputs for external events directly but receiving modulated information flow from the other nodes of the model, family-wise (dual: M1 and S1, versus single: S1 only). Bayesian model averaging implied that driving proprioceptive inputs were received S1 exclusively, however family-wise model selection was inconclusive in distinguishing the dual versus single input families. From the combination of sensory and motor gating incoming connections to the SMA our model of effective connectivity implies that sensorimotor integration as being a bidirectional convergence on the SMA. In a recent study, functional electrical stimulation altered proprioception and increased the influence of M1 on S1, which suggested that M1 should be considered as part of a sensorimotor hierarchy providing top–down proprioceptive predictions (Gandolla et al., 2014).

It is also notable that glove passive task activated M1 more and manual passive task activated S1 more, though both of the tasks are basically providing proprioceptive inputs in sensorimotor network (Song and Francis, 2013), the differences in the context sensitive influence on M1 and S1 would be characterized by the nature of each intervention. The nature of manual passive task delivered by a human assistant comprises more intense tactile stimulation and less predictable proprioception while that of glove passive task delivered by a soft robotic actuator comprises highly predictable proprioception (0.1 Hz) with less tactile intensity (Fig. 7C).

Based on the outcome of Bayesian model averaging (Fig. 7 B & C) the current model of effectivity connectivity implies that manual passive task preferentially drives the signal from S1 to SMA as well as contralateral S1 and subsequently fine-tunes M1 activity which will send reciprocal efferent signal to SMA. This feedback will modulate SMA according to proprioceptive input from S1. In this way, a real-time modulation of the motor command would be triggered by predictions of the sensory consequence of the movement and any discrepancy with the actual sensory feedback, in line with a predictive coding account of proprioceptive feedback for active motor control (van Beers et al., 2002; Bays and Wolpert, 2007; Franklin and Wolpert, 2011). Furthermore, the BMA results include nonlinear modulation by the M1 which imply that the highly predictable proprioceptive input produced by glove passive task that the efferent signal from M1 gates S1 signal heading to SMA. Together these gating mechanisms can explain M1-or S1-initiated feedback to the SMA-centered proprioceptive motor integration which may contribute to the generation of internal body representations required for movement monitoring (Sommer and Wurtz, 2008).

Though the effect of neurorehabilitation therapeutics, such as motor imagery, on neuroplasticity has been frequently explored, the effect of passive range of motion exercise therapy has been rarely investigated using functional imaging tools. From a clinical perspective, our fMRI study findings may present basic neurophysiological evidence regarding the mechanism of how the physiotherapy mobilizing paralyzed

extremities can change the brain metabolism to facilitate the recovery of motor function. The potential difference between conventional manual therapy and automated robotic therapy in the working process of proprioceptive motor integration was discussed.

Furthermore, due to the limited sample size, caution should be taken when making generalizations about the study findings, which should be addressed in future trials.

5. Conclusion

The present study demonstrates that proprioceptive inputs produced by a passive range of motion exercise can activate primary motor cortex and the supplementary motor area orchestrates the proprioceptive motor integration using the feedback mechanism. The Bayesian model selection suggests proprioceptive drive might influence primary motor cortex directly as well as indirectly via primary sensorimotor cortex activation and the subsequent modulation of the supplementary motor area.

Acknowledgements

This research was supported by National University Health System-Clinical Imaging Research Centre-Seed Funding, Singapore (R172-000-323-511) and Motor Accident Insurance Commission (MAIC), The Queensland Government, Australia (grant number: 2014000857).

Appendix A. Supplementary data

Supplementary data to this article can be found online at https://doi.org/10.1016/j.neuroimage.2019.116023.

Conflicts of interest

There are no conflicts of interest for any author.

Data and code availability

The code and the data used to produce the results reported in the manuscript are available on the official data repository of The University of Queensland (https://rdm.uq.edu.au/record/ROBH2019).

References

Akkal, D., Dum, R., Strick, P., 2007. Supplementary motor area and presupplementary motor area: targets of basal ganglia and cerebellar output. J. Neurosci. 27, 10659.
Asemi, A., Ramaseshan, K., Burgess, A., Diwadkar, V., Bressler, S., 2015. Dorsal anterior cingulate cortex modulates supplementary motor area in coordinated unimanual motor behavior. Front. Hum. Neurosci. 9, 309-309.
Bardouille, T., Boe, S., 2012. State-related changes in MEG functional connectivity reveal the task-positive sensorimotor network. PLoS One 7 (10), e48682.
Bays, P.M., Wolpert, D.M., 2007. Computational principles of sensorimotor control that minimize uncertainty and variability. J. Physiol. 578 (Pt 2), 387–396.
Behrens, T.J., Johansen-Berg, H., Woolrich, M., Smith, S., Wheeler-Kingshott, C., Boulby, P.,.
Bishop, R., 2014. Exploring the sensorimotor network using functional connectivity and graph theory. http://hdl.handle.net/10222/54014.
Breakspear, M., 2013. Dynamic and stochastic models of neuroimaging data: a comment on Lohmann et al. Neuroimage 75, 270.
Caparelli, E., Tomasi, D., Arnold, S., Chang, L., Ernst, T., 2003. k-Space based summary motion detection for functional magnetic resonance imaging. Neuroimage 20, 1411–1418.
Chung, G., Han, Y., Jeong, S., Jack, C., 2005. Functional heterogeneity of the supplementary motor area. AJNR (Am. J. Neuroradiol.) 26, 1819.
Cignetti, F., Fontan, A., Menant, J., Nazarian, B., Anton, J., Vaugoyeau, M., Assaiante, C., 2017. Protracted development of the proprioceptive brain network during and beyond adolescence. Cerebr. Cortex 27, 1285–1296.
Dum, R., Strick, P., 1991. The origin of corticospinal projections from the premotor areas in the frontal lobe. J. Neurosci. 11, 667.
Fischl, B., 2012. FreeSurfer. NeuroImage 62, 774–781.
Floyer-Lea, A., Matthews, P., 2004. Changing brain networks for visuomotor control with increased movement automaticity. J. Neurophysiol. 92 (4), 2405–2412.
Franklin, David W., Wolpert, Daniel M., 2011. Computational mechanisms of sensorimotor control. Neuron 72 (3), 425–442.
Friston, K., Harrison, L., Penny, W., 2003. Dynamic causal modelling. Neuroimage 19, 1273–1302.
Gandolla, M., Ferrante, S., Molteni, F., Guanziroli, E., Frattini, T., Martegani, A., Ferrigno, G., Friston, K., Pedrocchi, A., Ward S., N., 2014. Re-thinking the role of motor cortex: context-sensitive motor outputs? Neuroimage 91, 366–374.
Godfrey, S.B., Zhao, K.D., Theuer, A., Catalano, M.G., Bianchi, M., Breighner, R., et al., 2018. The Soft Hand Pro: Functional evaluation of a novel, flexible, and robust myoelectric prosthesis. PLoS ONE 13 (10), e0205653.
Grefkes, C., Nowak, D., Wang, L., Dafotakis, M., Eickhoff, S., Fink, G., 2010. Modulating cortical connectivity in stroke patients by rTMS assessed with fMRI and dynamic causal modeling. Neuroimage 50 (1), 233–242.
Greve, D., Fischl, B., 2009. Accurate and robust brain image alignment using boundary-based registration. Neuroimage 48, 63–72.
Haghshenas-Jaryani, M., Carrigan, W., Wijesundara, M., Patterson, R., Bugnariu, N., Niacaris, T., 2016. Kinematic Study of a Soft-And-Rigid Robotic Digit for Rehabilitation and Assistive Applications. The American Society of Mechanical Engineers, V05BT07A065.
Inase, M., Tokuno, H., Nambu, A., Akazawa, T., Takada, M., 1999. Corticostriatal and corticosubthalamic input zones from the presupplementary motor area in the macaque monkey: comparison with the input zones from the supplementary motor area. Brain Res. 833, 191–201.
Jack, D., Boian, R., Merians, A., Tremaine, M., Burdea, G., Adamovich, S., Recce, M., Poizner, H., 2001. Virtual reality-enhanced stroke rehabilitation. IEEE Trans. Neural Syst. Rehabil. Eng. 9, 308–318.
Jenkinson, M., Smith, S., 2001. A global optimisation method for robust affine registration of brain images. Med. Image Anal. 5, 143–156.
Jenkinson, M., Bannister, P., Brady, M., Smith, S.M., 2002. Improved optimization for the robust and accurate linear registration and motion correction of brain images. Neuroimage 17, 825–841.
Kahan, J., Foltynie, T., 2013. Understanding DCM: ten simple rules for the clinician. Neuroimage 83, 542–549.
Koh, T., Cheng, N., Yap, H., Yeow, C., 2017. Design of a soft robotic elbow sleeve with passive and intent-controlled actuation. Front. Neurosci. 11, 597-597.
Kuhtz-Buschbeck, J., Gilster, R., Wolff, S., Ulmer, S., Siebner, H., Jansen, O., 2008. Brain activity is similar during precision and power gripping with light force: an fMRI study. Neuroimage 40 (4), 1469–1481.
Liu, J., Morel, A., Wannier, T., Rouiller, E., 2001. Origins of callosal projections to the supplementary motor area (SMA): a direct comparison between pre-SMA and SMA-proper in macaque monkeys. J. Comp. Neurol. 443, 71–85.
Luppino, G., Matelli, M., Camarda, R., Rizzolatti, G., 1993. Corticocortical connections of area F3 (SMA-proper) and area F6 (pre-SMA) in the macaque monkey. J. Comp. Neurol. 338, 114–140.
Maier, R., Remus, U., 2002. Defining process-oriented knowledge management strategies. Knowl. Process Manag. 9, 103–118.
Mayka, M., Corcos, D., Leurgans, S., Vaillancourt, D., 2006. Three-dimensional locations and boundaries of motor and premotor cortices as defined by functional brain imaging: a meta-analysis. Neuroimage 31, 1453–1474.
Mitz, A., Wise, S., 1987. The somatotopic organization of the supplementary motor area: intracortical microstimulation mapping. J. Neurosci. 7, 1010.
Murray, E., Coulter, J., 1981. Organization of corticospinal neurons in the monkey. J. Comp. Neurol. 195, 339–365.
Orgogozo, J., Larsen, B., 1979. Activation of the supplementary motor area during voluntary movement in man suggests it works as a supramotor area. Science 206 (4420), 847.
Penfield, W., Welch, K., 1951. The supplementary motor area of the cerbral cortex; a clinical and experimental study. AMA Arch. Neurol. Psychiatr. 3, 289–317.
Penny, W., Stephan, K., Daunizeau, J., Rosa, M., Friston, K., Schofield, T., Leff, A., 2010. Comparing families of dynamic causal models. PLoS Comput. Biol. 6 (3) e1000709-e1000709.
Pollok, B., Gross, J., Dirks, M., Timmermann, L., Schnitzler, A., 2004. The cerebral oscillatory network of voluntary tremor. J. Physiol. 554 (Pt 3), 871–878.
Potgieser, A., de Jong, B., Wagemakers, M., Hoving, E., Groen, R., 2014. Insights from the supplementary motor area syndrome in balancing movement initiation and inhibition. Front. Hum. Neurosci. 8, 960-960.
Rigoux, L., Stephan, K., Friston, K., Daunizeau, J., 2014. Bayesian model selection for group studies — Revisited. Neuroimage 84, 971–985.
Smith, S., 2002. Fast robust automated brain extraction. Hum. Brain Mapp. 17, 143–155.
Sommer, M.A., Wurtz, R.H., 2008. Brain circuits for the internal monitoring of movements. Annu. Rev. Neurosci. 31 (1), 317–338.
Song, W., Francis, J.T., 2013. Tactile information processing in primate hand somatosensory cortex (S1) during passive arm movement. J. Neurophysiol. 110 (9), 2061–2070.
Stephan, K., Penny, W., Daunizeau, J., Moran, R., Friston, K., 2009. Bayesian model selection for group studies. Neuroimage 46, 1004–1017.
Stephan, K., Penny, W., Moran, R., den Ouden, H., Daunizeau, J., Friston, K., 2010. Ten simple rules for dynamic causal modeling. Neuroimage 49, 3099–3109.
Stock, A., Wascher, E., Beste, C., 2013. Differential effects of motor efference copies and proprioceptive information on response evaluation processes. PLoS One 8, e62335.
Tarvainen, T., Fernandez-Vargas, J., Yu, W., 2018. New layouts of fiber reinforcements to enable full finger motion assist with pneumatic multi-chamber elastomer actuators. Actuators 7.

van Beers, R.J., Baraduc, P., Wolpert, D.M., 2002. Role of uncertainty in sensorimotor control. Phil. Trans. R. Soc. Lond. Ser. B Biol. Sci. 357 (1424), 1137–1145.
Xia, M., Wang, J., He, Y., 2013. BrainNet viewer: a network visualization tool for human brain connectomics. PLoS One 8 (7), e68910.
Xu, L., Zhang, H., Hui, M., Long, Z., Jin, Z., Liu, Y., Yao, L., 2014. Motor execution and motor imagery: a comparison of functional connectivity patterns based on graph theory. Neuroscience 261, 184–194.
Yap, H., Kamaldin, N., Lim, J., Nasrallah, F., Goh, J., Yeow, C., 2017. A magnetic resonance compatible soft wearable robotic glove for hand rehabilitation and brain imaging. IEEE Trans. Neural Syst. Rehabil. Eng. 25, 782–793.
Zhang, H., Xu, L., Zhang, R., Hui, M., Long, Z., Zhao, X., Yao, L., 2012. Parallel alterations of functional connectivity during execution and imagination after motor imagery learning. PLoS One 7, e36052.